



commodity Wi-Fi, the source-defined obfuscation promoted by MIMOCrypt is superior to existing solutions in two other aspects, given that the decryption keys can be securely conveyed to legitimate users: on one hand, MIMOCrypt supports multi-user scenarios while thwarting unauthorized eavesdropping; on the other hand, the Wi-Fi communication quality can be largely retained for legitimate users.

Performing signal obfuscation always affects both communication and sensing for legitimate users, but this is a price to be paid for thwarting unauthorized eavesdropping.<sup>1</sup> Fortunately, MIMOCrypt’s source-defined channel encryption offers a full control on various parties, including both legitimate and unauthorized users, as well as users of both sensing and communication services. Consequently, the CSI encryption mechanism can be optimized so as to strike an adequate balance among i) risk of unauthorized eavesdropping, ii) legitimate sensing accuracy, and iii) communication quality. In addition, we propose an efficient decryption procedure for relatively coarse-grained sensing tasks such as user gesture and activity recognition driven by a deep neural model, exploiting the distinction between sensing and communication in required signal granularity.<sup>2</sup> In summary, we make the following major contributions in MIMOCrypt:

- We realize the first secure Wi-Fi sensing system for multi-user scenarios; it reconciles the conflict between thwarting unauthorized eavesdropping and maintaining service qualities to legitimate users.
- We propose a source-defined channel encryption scheme, in order to maintain compatibility with Wi-Fi while delivering a flexible control to meet the demands from various parties under the multi-user scenario.
- We explore a multi-objective optimization framework for designing the channel encryption scheme, aiming to strike an adequate balance among functions with conflicting targets.
- We propose a novel decryption procedure for sensing tasks leveraging deep learning; it can be made more efficient than its counterpart for communications.
- We implement a MIMOCrypt prototype based on WARP [21] and conduct extensive experiments upon it to demonstrate the efficacy of MIMOCrypt.

The rest of the paper is organized as follows. Section 2 sets up the background for the overall presentation before defining the attack model, discussing the related literature, and describing our brief solution. Section 3 uses simple experiments to motivate the design of MIMOCrypt, and Section 4 presents the design details. In these three sections, while describing the background, motivation, and workflow behind MIMOCrypt, we gradually formalize the mathematical models for general Wi-Fi sensing and for

1. Therefore, MIMOCrypt is not meant for all application scenarios; it should be deployed only where privacy sensitivity is high.

2. Fine-grained sensing tasks such as vital signs monitoring [20] are not considered in our context, as they often require rather short distances potentially exposing the eavesdroppers.

specific techniques under MIMOCrypt. Subsequently, Sections 5 and 6 respectively report the experiment setting and performance evaluation results of MIMOCrypt. We then discuss the limitations in Section 7 and finally conclude our paper in Section 8. We postpone extended security analysis, several details on parameter settings, as well as future works to the Appendices.

## 2. BACKGROUND AND LITERATURE

In this section, we provide basic knowledge on Wi-Fi sensing and define the attack model to characterize the potential risk of privacy leakage. We then discuss more on the literature based on explained basics and model. Finally, we briefly introduce the key rationale behind our solution.

### 2.1. Wi-Fi Sensing and CSI

During a multipath propagation process, Wi-Fi signals may experience diversified distortions determined by environment (hence channel) conditions. In particular, a moving object can substantially alter the signal propagation environments and thus the Wi-Fi channels. For instance, performing gestures between a pair of Wi-Fi transmitter and receiver can block certain signal paths while generating new ones, thereby causing the corresponding variations in Wi-Fi channels. In other words, the foundation of Wi-Fi sensing is the correlation between Wi-Fi channel variations and the states of moving objects.

While enabling sensing, Wi-Fi channel (i.e., CSI) estimation is also the default key to decode communication symbols. Therefore, existing Wi-Fi standards heavily rely on preambles (in particular the *long training sequence* (LTS) [22] contained inside) for performing CSI estimations and in turn for correctly decoding the communication symbols. Wi-Fi LTS is a piece of known yet unalterable information without any encryption [23], so anyone (regardless of whether registered to a Wi-Fi network or not) can potentially leverage a device equipped with Wi-Fi NICs (network interface cards) to overhear the LTSs and extract the CSI passively. When a Wi-Fi transmitter (Tx) sends an LTS signal  $s_{n,m}$  at the  $n$ -th OFDM subcarrier (cardinality  $N$ ) of the  $m$ -th packet (cardinality  $M$ ), the receiving (Rx) signals become  $y_{n,m} = h_{n,m}s_{n,m}$  where the CSI  $h_{n,m}$  is obtained as  $h_{n,m} = y_{n,m}/s_{n,m}$ . To facilitate estimating  $h_{n,m}$ ,  $s_{n,m}$  actually remains constant in  $m$ . According to [24],  $h_{n,m}$  can be modeled as:

$$h_{n,m} = \sum_{k=1}^K \alpha_{n,m,k} e^{-j2\pi(f_c + n\Delta f)\tau_{m,k}} \quad (1)$$

where  $\alpha_{n,m,k}$  is the attenuation along the  $k$ -th path,  $f_c$  denotes the carrier frequency,  $\Delta f$  represents the subcarrier spacing, and  $\tau_{m,k} = \tau_k^S + \tau_{m,k}^D$  refers to the time delay: the static one  $\tau_k^S$  from an arbitrary reflector and the dynamic one  $\tau_{m,k}^D$  caused by its motions.

Given a CSI matrix  $H_q = [h_{n,m}]_q$  from the  $q$ -th Tx antenna, the in total  $Q$  ( $Q = 8$  for a 8 Tx antenna case) CSI

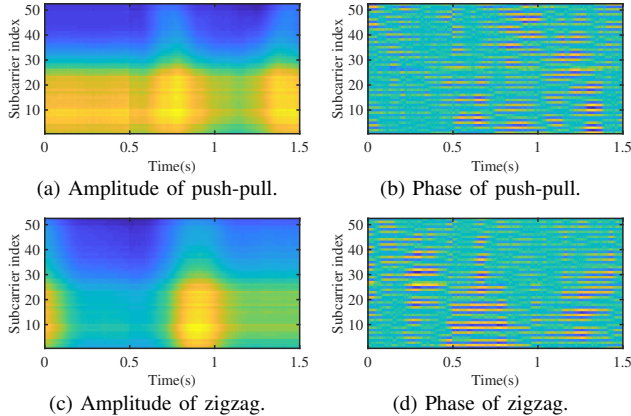


Figure 2: CSI amplitudes and phases of two common gestures, while (a)-(b) of “push-pull” and (c)-(d) of “zigzag”.

matrices offers a substantial amount of information on the status and variations of the ambient environments; they have thus enabled a wide spectrum of Wi-Fi sensing applications, including activity tracking [4], indoor localization [7], and gesture recognition [10]. Although targeting distinct sensing goals, these proposals all rely on features extracted from CSI, i.e., amplitudes and phases of individual subcarriers, as well as their variations across time  $m$  and frequency  $n$ . Since the aggregated amplitude of all subcarriers (a.k.a. RSSI) used by earlier proposals [17], [18] is merely a low-end variant of CSI, we focus on preserving privacy for CSI-enabled Wi-Fi sensing throughout our paper. To further illustrate the correlations between CSIs and user motion states, we take gesture recognition as an example. Figure 2 presents CSI amplitudes and phases of all subcarriers and across several LTSs upon performing two hand gestures: push-pull and drawing a zigzag. We can clearly observe the distinctions in CSI features between the two gestures, so these results indicate the feasibility of using CSI features to differentiate user motion states. To simplify our design, we decide to protect all subcarriers as a whole by imposing distinct “scrambling” in time. Consequently, we omit the frequency dimension  $n$  from now on.

## 2.2. Attack Model

As mentioned earlier, no encryption is applied to Wi-Fi LTS, hence anyone with a Wi-Fi NIC can potentially overhear the CSIs from various APs around it, even without being registered (hence authenticated). We consider a *multi-user scenario* where an AP (Alice) can thwart multiple eavesdroppers (Eves, albeit only one is shown in Figure 1), while maintaining services to multiple legitimate sensing and communication users Bob<sup>S</sup> and Bob<sup>C</sup>. As an eavesdropper, Eve appears to be common users with Wi-Fi NICs in possession and bear in mind *stealthiness* when launching attacks. To maintain the stealthiness, an Eve performs *passive* Wi-Fi sensing by acquiring CSI vector  $\mathbf{h} = [\mathbf{h}_m]$  from an

AP (Alice) without being registered to it,<sup>3</sup> and thus eavesdrops on private information of close-by persons (*victims* who are not necessary Wi-Fi users), such as their password inputs and/or control gestures. To remain focusing on the defending scheme, only *hand gesture recognition* (HGR) task is considered throughout the paper, yet our proposal is readily extensible to defend other sensing tasks. Moreover, Bobs and Eves adopt a publicly-known neural model (e.g., WiSee [25]) to perform HGR. Finally, the AP (Alice) is always deemed as a trusted party, so security issues such as rogue APs [16], [26] are not our concern. Specifically, our attack model endows Eve with the following capabilities stronger or at least equal to existing ones [15]:

*Eavesdropping Position.* We do not impose any physical limitations on Eves’ positions. In particular, Eves and Bobs do not have to be separated into different physical spaces; this differs significantly from existing proposals [17], [18], [27] to be elaborated in Section 2.3. Essentially, we allow Eves to choose any proper positions to maximize their chance of eavesdropping while still maintaining stealthiness.

*Antenna Quantity.* Considering the hardware configuration of common Wi-Fi NICs (e.g., those used by smartphones and laptops) and the stealthiness required by Eve, we assume that Eve is equipped with two antennas [28]. However, to demonstrate the strength of our proposal in thwarting more powerful eavesdropping capabilities, we use both security analysis in Section 4.3 and experiments in Section 6.3.3 to confirm that increasing antenna numbers does not make the attack model stronger.

*Multiple Attackers.* We allow multiple Eves to collude with each other, so as to increase the number of antennas under their possession. However, the stealthiness of Eves forbid them to collude in the form of launching *known-plaintext attack* (KPA). Since the information (hence the *plaintext*) to be protected under our model is a *physical process* of hand gesture, launching KPA requires the *physical presence* of at least two Eves in the service range of the AP: one acts as the victim to generate physical plaintexts (hand gestures) and another observes the resulting CSI variations. Nonetheless, such an obvious attack would severely expose Eves and hence totally go against their stealthiness.

*HGR Model.* To follow the *open design principle* that the security of a mechanism should not depend on the secrecy of its design or implementation, we let Bobs and Eves share the same HGR model readily retrievable from certain public domains. In our evaluations, common HGR models Widar3 [10] and WiSee [25]) are adopted to quantify the effectiveness against malicious eavesdropping.

## 2.3. Existing Solutions

Given the attack model defined in Section 2.2, Qiao *et al.* propose PhyCloak [15] as one of the seminal countermeasure to thwart such eavesdropping attacks. Essentially,

3. As both Eve and Bob<sup>S</sup> act passively, only one instance needs to be considered in performance evaluation.

PhyCloak assumes an HGR setting similar to Figure 1 but, instead of multiple legitimate users (Bobs) and unauthorized eavesdroppers (Eves), only one Bob is allowed and all others are deemed as Eves. Therefore, PhyCloak lets Bob to first perform sensing and then obfuscate the channel  $\mathcal{h}_m$  so as to prevent Eves from doing the same. To perform these two tasks simultaneously (otherwise Eves can still perform sensing before the arrival of obfuscated signals), sophisticated yet immature FDR [29] was adopted. While PhyCloak apparently cannot support multiple legitimate users, the need for FDR has substantially increased the system complexity and made PhyCloak incompatible with Wi-Fi standard. Though the experiments of PhyCloak show that it barely affects communication quality, one would suspect the results of being biased because, as far as Bob sufficiently scrambled  $\mathcal{h}_m$ , communication quality is almost surely affected, albeit to a little less extent than Eves’ sensing.

A similar idea of obfuscating the channel  $\mathcal{h}_m$  has been further extended in Aegis [27] and it also aims to defend HGR, so all the aforementioned drawbacks of PhyCloak are inherited by Aegis. The only difference is that Aegis involves a motorized platform so that obfuscating  $\mathcal{h}_m$  is achieved by changing the speed and direction of Bob’s antennas. Recently, IRshield [18] considers the more aggressive scenario deeming everyone to be an Eve, which has significantly simplified the solution. Basically, IRShield adopts customized IRSs [30] installed beside an AP to obfuscate  $\mathcal{h}_m$ . As a result, no one can perform CSI-based sensing anymore, yet communication quality should also be affected, though the experiments (with only one link) seem to suggest a negligible level of variation. Clearly, *direct channel obfuscation* is impractical since it lacks necessary controllability to differentiate between legitimate users (of both sensing and communications) and eavesdroppers.

To better control the channel obfuscation, one may consider scrambling  $\mathcal{s}_m$  so that the derived  $\mathcal{h}_m = \mathcal{y}_m/\mathcal{s}_m$  gets obfuscated. As  $\mathcal{s}_m$  can be fully controlled by Alice (an AP), differentiating “good or evil” in a multi-user scenario becomes possible. As a primitive version of this *source-defined channel scrambling* approach, [17] dynamically adjusts the Tx power to scramble the amplitude of  $\mathcal{h}_m$ . Since CSI phases  $\tau_k$  are not affected, this solution only works for certain sensing tasks such as (rough) indoor localization. Jiao *et al.* [31] leverages a secret switching sequence among a set of pre-defined LTSs to perform scrambling upon  $\mathcal{s}_m$ . Such a solution is surely impractical because LTS is fixed in the digital circuit of an Wi-Fi NIC; it can be altered in [31] only thanks to the adoption of customized hardware. Also, the binary pattern of LTS offers very little scrambling space.

#### 2.4. Rationale behind Our Solution

According to the aforementioned discussions, a distinction between normal (communication) security and sensing security becomes evident: the former has *digital* plaintexts while those of the latter are *physical*. This has made existing

sensing security solutions (wrongly) believe that arbitrary scrambling (sacrificing Bobs) could be the only solution to thwart eavesdropping attacks. Fortunately, we can formally encrypt them (albeit physically) instead, so as to thwarts Eves without harming Bobs. Recalling that digital encryption widely used for data protection, such as advanced encryption standard (AES) [32], essentially leverages cryptographic keys to digitally “modulate” plaintexts. The same idea of “modulation for encryption” can be applied to physical plaintexts, though it may require a combination of digital control and physical execution. In particular, though LTS cannot be altered, we may exploit (digital) Wi-Fi MIMO beamformers [33] to physically change the transmitted form of LTS: as far as the sequence of beamformers (equivalent to a cryptographic key) are kept secret, our physical plaintexts are successfully encrypted and thus hidden from Eves with no knowledge of the key. It is worth noting that the idea of *encrypting physical plaintext* differs fundamentally from the *physical layer security* mechanisms meant to protect only *digital plaintext* without a cryptographic key [34]–[36].

### 3. MOTIVATIONS & FEASIBILITY STUDY

We hereby leverage simple experiments to further motivate the design of MIMOCrypt, while verifying its feasibility.

#### 3.1. Thwarting Eavesdroppers

As discussed in Section 2.2, an eavesdropper stealthily obtains the CSI vector from an AP, so as to extract gesture-dependent features and perform HGR for inferring the private information of another person. Let us briefly demonstrate how MIMO beamformers can encrypt CSIs [ $\mathcal{h}_m$ ] (hence the gestures) to thwart the eavesdroppers. Essentially, an *encryption matrix*  $\Psi$  is applied to scramble an LTS vector  $\mathcal{s} = [\mathcal{s}_m]$ : since  $\mathcal{s}_m = 1, \forall m$  without loss of generality (see Section 2.1), the outcome  $\mathcal{s}' = \mathcal{E}(\mathcal{s}, \Psi)$  leads to an encryption of [ $\mathcal{h}_m$ ] as  $\mathcal{h}_m = \mathcal{y}_m/\mathcal{s}'_m$ . Consequently, Eves would fail to eavesdrop HGRs without the knowledge of  $\Psi$ . To ease the exposition of the encryption procedure  $\mathcal{E}(\cdot)$ , we hereby give a simple case study of transmitting an LTS vector  $\mathcal{s} = [\mathcal{s}_m]_{1 \leq m \leq M}$  with 8 Tx antennas. Specifically, the component in  $\Psi$  for each time instance  $m$  are 8 complex values (corresponding to the 8 antennas); they are multiplied to 8  $\mathcal{s}_m$ ’s (actually just 1’s) individually and then get randomly and independently altered for  $m + 1$ . Finally, the 8 independently scrambled [ $\mathcal{s}'_{m, 1 \leq q \leq 8}$ ] are transmitted *simultaneously* via 8 Tx antennas of Alice and then received by each Rx antenna of Bobs or Eves after these transmissions (via 8 independent channels) get mixed in the air.

We set up an experiment using two combined WARP nodes with 8 antennas to act as Alice, and another WARP node with 1 antenna as Eve. The distance between them is set to 3.5 m, while one victim waves a hand along a “zigzag” path at 0.5 m distance from Alice. We extract

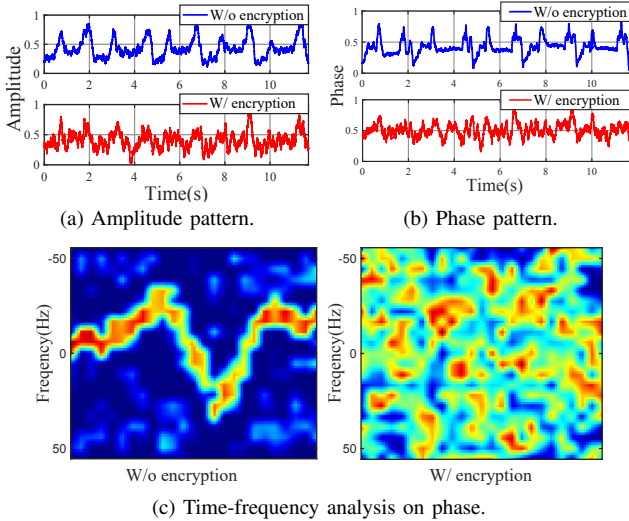


Figure 3: CSI sensing results of “zigzag” hand waving. Results with/without MIMO encryption appear in forms of (a) amplitude, (b) phase, and (c) time-frequency analysis.

CSI features from one randomly selected subcarrier (the 32-th in this case) for illustration purpose. The amplitude and phase variations of this subcarrier induced by the hand gesture with or without applying  $\Psi$  are respectively shown in Figures 3a and 3b; we further perform time-frequency analysis on the phases to derive Figure 3c. Apparently, while the CSI can clearly “depict” the zigzag hand gesture (with two peaks indicating the turning points of the motion path), such critical information gets totally deprived of from the CSI after applying  $\Psi$ .

### 3.2. Communications for Legitimate Users

Applying the encryption matrix  $\Psi$  is a double-sided sword: since it scrambles the CSIs to all potential receivers, it hurts both eavesdroppers and legitimate users (both Bob<sup>C</sup> and Bob<sup>S</sup>). We hereby use a simple experiment to showcase the degradation of communication quality, judged by the commonly adopted SNR (signal-to-noise ratio) metric. To effectively measure this metric, we fix the antenna gain of the 8-antenna WARP node to 3 dBi and the transmission power of radio-frequency (RF) front-end to 20 dBm. We let the node (Alice) transmit 1000 data packets with encrypted LTS, while another 1-antenna node (Bob) observes the SNR distribution of the Rx LTS signals. As depicted in Figure 4a, the average SNR is only 4.81 dB, less than the required threshold: Wi-Fi network normally demands at least a 5 dB SNR, below which even the error rate of LTS (using BPSK) can be drastically increased [37]. Meanwhile, the payload (no  $\Psi$  applied) also suffers as shown by the two leftmost curves in Figure 4b, because correct CSIs (estimated from LTS’s) are crucial to communication qualities.

Fortunately, initiating the MIMO encryption by an AP (thus our source-defined concept) provides a natural leverage

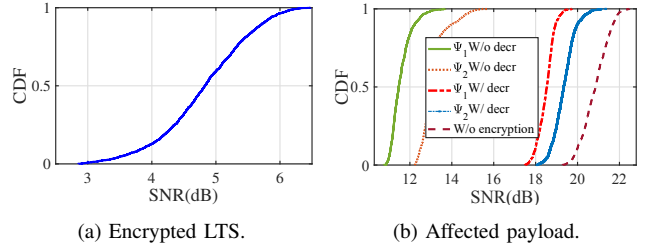


Figure 4: Channel encryption significantly degrades the Rx quality for LTS indicated by SNR (a) and affects the Rx quality of the payload (b). Though decrypting LTS may counteract the loss in payload SNR (b), the extent of compensation vary given different encryption matrices  $\Psi$ ’s.

to handle this problem: legitimate users can decrypt the CSIs with  $\Psi$  securely conveyed to them. This is in stark contrast to prior channel obfuscation approaches lacking of ability to distinguish between Eves and Bobs [15], [18]. Nevertheless, owning  $\Psi$  does not directly lead to the recovery of true CSIs, because the encryption may cause higher CSI estimation errors due to the twisted waveform (to be elaborated in Section 4.4). We choose two arbitrary  $\Psi$ ’s to share between Alice and Bob; observations made on the SNR distributions of payload in Figure 4b are: i) though significantly elevated compared with no LTS decryption, the average SNRs are still below that of normal Wi-Fi communications, and ii) the SNR distributions corresponding to the two arbitrary  $\Psi$ ’s bear discernible differences, indicating a chance of further improving the SNR by selecting the optimal  $\Psi$ ’s. In summary, while optimizing  $\Psi$  is crucial to protecting legitimate users, our source-defined MIMO encryption scheme offers a handle to approach the optimization problem involving multiple objectives: namely thwarting eavesdroppers while still preserving the service quality for legitimate users.

### 3.3. Efficient Sensing for Legitimate Users

Although Bobs can perform both communication and sensing tasks by first decrypting the received CSI, there might exist more efficient ways to execute the sensing tasks. In particular, a straightforward implementation of HGR under MIMO encryption with  $\Psi$  is to first recover the true CSI vector  $[\mathcal{L}_m]$  and then feed it into a trained neural model (e.g., [10], [38]). Nevertheless, this process involves the inversion of  $\Psi$  and additional matrix computations, thus resulting in extra time costs that cannot be ignored for resource-limited Bobs. Fortunately, as sensing tasks often demand a lower signal granularity than communication tasks, explicitly inverting  $\Psi$  can be avoided. Basically, whereas communications have to recover symbols represented by every Rx frame, HGR only requires differentiating a countable amount of gestures given multiple Rx frames. Therefore, a light-weight implementation could rely on a neural model to concurrently handle both  $\Psi$ -related operations and HGR.

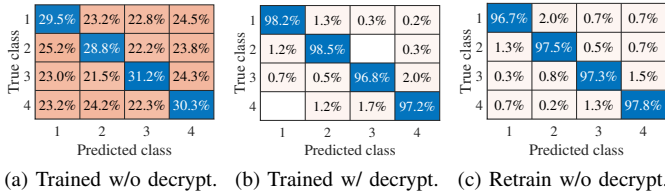


Figure 5: HGR performance under different training and inputs: (a) a *trained* model with encrypted CSIs, (b) the *trained* model with decrypted CSIs, and (c) a *retrained* model with encrypted CSIs.

We hereby briefly verify the feasibility of the aforementioned two HGR strategies. We first collect a dataset with 12,000 CSI samples (each sample contains 2 s recording of CSI vector) of four common gestures (i.e., zigzag, circle, push, and clap) under both encrypted and decrypted cases, 80% of which are used for training an HGR model while the remaining part for testing the HGR performance. We adopt the HGR model in [10] as the basis, but we either directly use the trained model with both encrypted and decrypted CSIs as inputs, or retrain the model using the encrypted CSIs. As expected, Figures 5b and 5c demonstrate that the models taking  $\Psi$  into account (by either decrypting or retraining) perform much better than that with encrypted CSIs as input in Figure 5a. Moreover, the two well-performed strategies achieved very similar average accuracy of around 97%, but obtaining the decrypted CSIs requires an extra time consumption of 0.83 ms on the Snapdragon 8 Gen-1 CPU of a Xiaomi 12 smartphone. In reality,  $\Psi$  can be updated (similar to the security key update [39], [40]), so retraining an HGR model upon each update is highly impractical; incurring a minimal cost in updating  $\Psi$  is desirable.

## 4. MIMOCrypt: Derivation and Design

This section presents the theoretical derivations and technical workflow of MIMOCrypt. We first introduce a new metric to measure the Wi-Fi sensing quality for HGR (based on the well-known SNR metric for communications) in Section 4.1. Then we present the core design of MIMOCrypt in terms of spatial-temporal MIMO encryption in Section 4.2, followed by the security analysis in Section 4.3 and  $\Psi$  fine-tuning via a multi-objective optimization framework in Section 4.4. Finally, we propose an adaptive inference architecture (for Bob<sup>S</sup>) to accommodate encrypted CSIs with minor communication overhead in Section 4.5, before summarizing the workflow of MIMOCrypt in Section 4.6.

### 4.1. Quantifying Motion Sensing Quality

To have a security measure for the physical plaintext, we leverage SNR to quantify *relative entropy* [41], [42]. Though SNR is a well-known indicator for signal quality in communications, we need to refine it so as to suit the sensing task. Since Wi-Fi sensing (in particular HGR in our case)

mainly focuses on motions, we modify the SNR definition to quantify the ratio between Wi-Fi (motion) sensing signal and other non-signal components. Based on Eqn. (1), we have the *sensing SNR* represented as follows:

$$\eta_S = \frac{1}{M} \sum_{m=1}^M \frac{|\hat{h}_m^D|^2}{|\hat{h}_m^S|^2 + \sigma^2}, \quad (2)$$

where  $\sigma^2$  is the variance of Gaussian white noise. We denote the dynamic reflection channels caused by human motion as  $\hat{h}_m^D = \sum_{k \in K_D} \alpha_{m,k}^D e^{-j2\pi f_c \tau_k^D}$  and the static reflection channels from the surrounding objects (e.g., walls and furniture) as  $\hat{h}_m^S = \sum_{k \in K_S} \alpha_{m,k}^S e^{-j2\pi f_c \tau_k^S}$ . According to Eqn. (2), a large  $\eta_S$  indicates a stronger dynamic reflection signals over non-signal components, potentially resulting in better sensing performance.

As signal distortion caused by MIMO encryption is not considered in Eqn. (2), we hereby introduce a novel *signal-to-distortion-plus-noise ratio* (SDNR):

$$\eta_{SD} = \frac{1}{M} \sum_{m=1}^M \frac{|\hat{h}_m^D|^2}{|\hat{h}_m - \hat{h}_m|^2 + |\hat{h}_m^S|^2 + \sigma^2} \quad (3)$$

where  $\hat{h}_m$  is the encrypted CSI, and  $|\hat{h}_m - \hat{h}_m|^2$  represents the distortion caused by MIMO encryption: it also indicates a gain in entropy. We conduct experiments with the same settings adopted in Section 3.1, and we calculate the  $\eta_{SD}$  of original and encrypted CSIs (via 4 encryption matrices  $\Psi$ 's to be elaborated in Section 4.2), while leveraging cosine similarity to compare their signal envelopes. The results in Figure 6 reveal two critical points: i)  $\eta_{SD}$  and signal similarity share the same variation trend, hence confirming SDNR's effectiveness, ii) encryption indeed works but to different extents determined by  $\Psi$ , so we can further optimize  $\Psi$ 's to fine-tune the encryption strength in Section 4.4.

### 4.2. Spatial-Temporal Encryption

According to Section 3.1, applying an encryption matrix  $\Psi$  to Wi-Fi LTS can largely thwart the Eve's intention to infer privacy-sensitive information via Wi-Fi sensing. To better characterize our source-defined channel encryption, we hereby consider only one Wi-Fi NIC (either Bob or Eve) when presenting MIMOCrypt's encryption operations; the derivations can be readily extended to cover multiple NICs

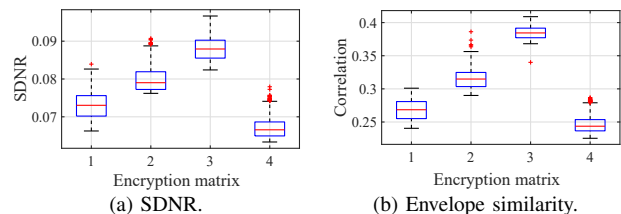


Figure 6: Four distinct  $\Psi$ 's lead to (a) SDNRs of encrypted CSIs and (b) CSI envelope similarities different from non-encrypted ones; (a) and (b) are very similar in trend.

due to Wi-Fi’s broadcast and time-division nature. How to differentiate Bob and Eve shall be discussed later, as the encryption operation deems them equally.

*MIMO-Driven Spatial-Temporal Encryption.* Let us formally present the source-defined encryption scheme in terms of the interaction between channels (or CSIs) and the encryption matrix  $\Psi$ . Essentially, the distorted CSIs observed by a single Rx antenna (of Bob or Eve) can be written as:

$$\hat{\mathbf{h}} = [\mathbf{h}_1, \dots, \mathbf{h}_q, \dots, \mathbf{h}_{Q^{\text{Tx}}}] \Psi \quad (4)$$

where  $\Psi = [\Psi_1, \dots, \Psi_q, \dots, \Psi_{Q^{\text{Tx}}}]^T$ :  $\Psi_q = \text{diag}(\mathcal{d}_m)_q$  is an  $M \times M$  beamformer matrix applied to the  $q$ -th Tx antenna and  $\mathcal{d}_m$  is a complex value distinct to the  $m$ -th packet (CSI). We have  $\Psi_q = I$  (identity matrix) or  $\mathbf{0}$  without encryption, depending on whether the  $q$ -th antenna is used to transmit signals or not. Essentially, encrypting a time sequence of  $M$  CSIs leads to a *key length* of  $M$ , while the (implied) summation in Eqn. (4), indicating a “(in the air) spatial mix” of all  $Q^{\text{Tx}}$  transmissions, is similar to the MixColumns operation unique to AES [32], which makes the AES secure against the differential and linear cryptanalysis.

Without proper decryption, the degradation in the sensing performance of Eve can be characterized as, given the SDNR metric defined in Eqn. (3):

$$\eta_{\text{SD}}^{\text{Eve}} = \frac{1}{Q^{\text{Tx}}M} \frac{\|\hat{\mathbf{h}}^{\text{D}}\|_2^2}{\|\mathbf{h} - \hat{\mathbf{h}}\|_2^2 + \|\mathbf{h}^{\text{S}}\|_2^2 + \sigma^2}, \quad (5)$$

where the operation  $\|\cdot\|_2$  denotes the  $l^2$  norm. To verify the relation between  $\eta_{\text{SD}}$  (affected by encryption) and HGR sensing accuracy, we repeat the earlier experiments but adjust the distance between Alice and Eve from 2.5 to 5.2 m with a step size of 0.3 m. The victim then performs gestures at each Alice-Eve distance while the corresponding  $\eta_{\text{SD}}$  and HGR accuracy are measured. Figure 7 presents the average  $\eta_{\text{SD}}$  and HGR accuracy at the ten distinct Alice-Eve distances; it demonstrates a strong correlation between them, hence proving the effectiveness of  $\eta_{\text{SD}}$  in qualifying the sensing quality of Wi-Fi-based HGR, as well as the strength of  $\Psi$  in thwarting potential eavesdropping.

*Temporal Randomization.* As the spatial-temporary encryption enforced via  $\Psi$  assumes regular time intervals, the encryption strength can be further enhanced by randomizing the temporal dimension, because neural models

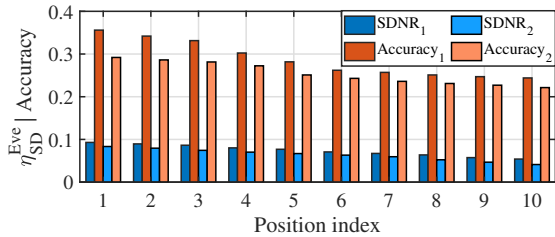


Figure 7: Hand gesture recognition accuracy under two  $\Psi$ ’s and varying SDNR  $\eta_{\text{SD}}$  measured at ten positions.

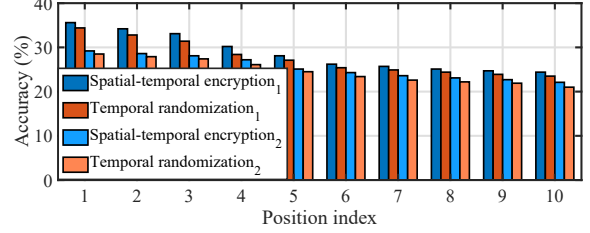


Figure 8: Hand gesture recognition accuracy under spatial-temporal encryption and temporal randomization.

are often trained under the assumption of a known and constant input interval. To perform temporal randomization, we let the packet intervals take irregular values  $\hat{t}_m = (m + \beta_m)\Delta t$  where  $\Delta t$  is the original (constant) interval and  $\beta_m \in [-0.5, 0.5]$  is the randomization ratio for the  $m$ -th packet. Consequently, the irregular interval time vector  $[\hat{t}_m]$  (unknown to Eve) forces Eve to use a pre-trained neural model to handle the encrypted CSIs with further tampered Doppler frequency shift patterns. We specifically evaluate whether the packet interval randomization can enhance the encryption strength of  $\Psi$ , reusing the previous experiment setting but under two cases: i)  $\Psi$  only, and ii) adding temporal randomization. Then we leverage a model trained with authentic CSIs (see Section 3.3) to perform HGR for the two cases. As shown in Figure 8, temporal randomization can further degrade HGR accuracy compared with that of  $\Psi$  only, especially at a closer distance.

### 4.3. Security Analysis

This analysis focuses on two major threats: the observation diversity of Eves and the side-channel KPA. We postpone extended discussions to Appendix A.

*Observation Diversity.* As Eve is totally unaware of the complex-valued parameters involved in  $\Psi$  whose quantity is  $Q^{\text{Tx}} \times M$ , it may attempt to gain more “observations” via different antennas (including antennas from colluded Eves) to somewhat remove  $\Psi$ . This diversity gain works under normal situation as the channel  $\mathbf{h}_m$  is the only known fact in  $\mathbf{h}_m = \mathbf{y}_m/\mathbf{s}_m$  for Rx decoding. However, MIMOCrypt encrypts the channels with  $\Psi$  as indicated by Eqn. (4). As a result, every new antenna Eve adds to its possession introduces  $Q^{\text{Tx}}$  new unknown parameters (the channels between AP’s antennas and that of Eve’s), while  $\Psi$  remains unknown. Consequently, we may surely conclude that Eve earns no diversity gain by adding more antennas.

*Side-channel KPA.* Although our attack model in Section 2.2 forbids full-scale KPAs, one may wonder if a few gesture samples serve as “side-channel” to break the encryption; a digital version of this attack was proposed by [35] leveraging partial plaintext such as protocol headers. In fact, this side-channel KPA has been thwarted by a *moving target defense* [36] that changes its (orthogonal) blinding patterns via physical antenna manipulations. Be-

cause MIMOCrypt adopts a cryptographic key whose beamformer patterns allow for much diversified choices from full space, side-channel KPA should not be a concern. In fact, this attack barely causes loss in conditional entropy, since  $\eta_{SD}^{Eve}$  in Eqn. (5), evaluated in statistical mean sense over a large amount of samples, cannot be significantly altered due to the exposure of a few samples; we shall further elaborate on this issue in both Section 7 and Appendix A. Unfortunately, the combination of physical encryption and physical plaintext also makes common security analysis on encryption schemes unsuitable: the encryption process is very different since complex operations are involved (i.e., beamformers comprise complex numbers) instead of digital substitution and transposition.

#### 4.4. Balancing Security and Performance

Whereas Section 4.2 indicates that the encryption of MIMOCrypt deems Bobs and Eves equally, their inherent difference can still be signified: Alice securely (re-)distributes the encryption matrices  $\Psi$ 's to Bobs (who have registered to the Wi-Fi network), which can be readily achieved via key distribution mechanisms [43]. Recalling that arbitrarily applying  $\Psi$ 's may degrade the communication quality for Bobs (see Figure 4 in the Section 3.2), since the tolerance range for CSI estimation errors [44] can be violated by scrambling, which we further illustrate using Figure 9. Because the same issue exists for Bobs performing sensing too, we hereby propose a *multi-objective optimization framework* to strike a balance among i) risk of eavesdropping, ii) communication quality, and iii) sensing accuracy. In forming the optimization, Alice relies on the standard feedback [45] from Bobs to obtain their CSIs, while estimating those for Eves by averaging the received feedback.

Since a good tradeoff among thwarting eavesdropping, enhancing (legitimate) sensing accuracy, and preserving communication quality cannot be achieved by a single objective, we model this tradeoff via a multi-objective optimization problem with the encryption matrix  $\Psi$  as the variable:

$$\max_{\Psi} [-\eta_{SD}^{Eve}, \eta_C^{Bob}, \eta_{SD}^{Bob}] \quad (6)$$

$$\text{s.t. } \|\Psi\|_2^2 \leq MQ^{Tx}, \quad (7)$$

$$\eta_C^{Bob} \geq \epsilon_C, \quad \eta_{SD}^{Bob} \geq \epsilon_{SD}, \quad (8)$$

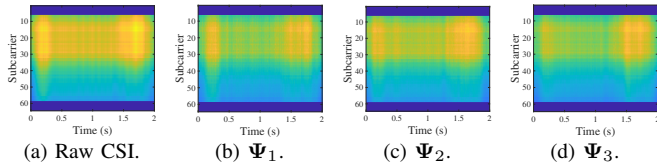


Figure 9: CSI distortion persists even with the inverse of  $\Psi$  for decryption. We hereby compare a raw CSI sample (a) with three encrypted and then decrypted versions (corresponding to three distinct  $\Psi$ 's) (b)-(d).

where the constraint (7) bounds the total power from above,  $\epsilon_C$  and  $\epsilon_{SD}$  in the constraint (8) act as the lower-bounds for the performance of Bob<sup>C</sup> (legitimate communication users) and Bob<sup>S</sup> (legitimate sensing users), respectively. The symbol  $\eta_C^{Bob} = \|\tilde{\mathbf{h}}\|_2^2/\sigma^2$  is the communication SNR of Bob<sup>C</sup>, and  $\eta_{SD}^{Bob}$  is the SDNR of Bob<sup>S</sup>: a revision to Eqn. (5) as decryption is applied here:

$$\eta_{SD}^{Bob} = \frac{1}{Q^{Tx}M} \frac{\|\tilde{\mathbf{h}}^D\|_2^2}{\|\Psi_q^{-1}\sigma\|_2^2 + \|\tilde{\mathbf{h}}^S\|_2^2 + \sigma^2}, \quad (9)$$

where  $\Psi^{-1}$  is the inverse of  $\Psi$ ,  $\tilde{\mathbf{h}}^D$  and  $\tilde{\mathbf{h}}^S$  are the dynamic and static reflection channels from Alice's Tx antennas to Bob's Rx antenna after decryption. The term  $\|\Psi^{-1}\sigma\|_2^2$  indicates that there still exists a *residue distortion*, as we have illustrated in Figure 9. Another observation to be drawn from Figure 9 is that, comparing with the original CSI, different  $\Psi$ 's lead to distinct residue distortions, hence the need for optimization over  $\Psi$ .

To locate a good tradeoff on the Pareto optimal frontier of the above optimization problem, we apply the scalarization trick via a set of weights [46]:

$$\max_{\Psi} \omega_1\eta_C^{Bob} + \omega_2\eta_{SD}^{Bob} - \omega_3\eta_{SD}^{Eve} \quad (10)$$

$$\text{s.t. } (7), (8), \sum_i \omega_i = 1, \quad (11)$$

where  $\omega_i \in [0, 1]$  is the scalar weight applied to an objective in the original problem (6). To solve the problem (10), we leverage ADMM [47] to obtain local optimal solutions of this nonlinear non-convex optimization. We omit the optimization for temporal randomization as this part does not affect the performance of Bobs.

*Remarks:* We deliberately put the optimization after the security analysis, because optimizing  $\Psi$  does not violate any arguments made in Section 4.3, hence it has virtually no impact on the encryption strength of  $\Psi$ .

#### 4.5. Sensing under Encrypted CSIs

According to Section 3.3 and 4.4, Bobs can perform both communication and sensing after receiving the securely distributed  $\Psi$  from Alice. Nonetheless, whereas this is necessary for Bob<sup>C</sup> and its overhead can be amortized over the large volume of data traffic, direct decryption for Bob<sup>S</sup> appears to be neither efficient nor necessary, because learning HGR can be conducted in the encrypted domain. In particular, as sensing tasks often demand a lower signal granularity than communication tasks (as explained in Section 3.3), we may build a deep sub-model to filter the encrypted CSIs so that they can correctly drive a given HGR model to perform classification. Though this sub-model pre-distributed to Bobs upon their registration still demands a *decryption key* to act on a specific  $\Psi$ , this key should incur a much lower overhead than  $\Psi$ .

*HGR Pipeline Given Encrypted CSIs.* Our HGR pipeline under MIMOCrypt framework comprises two major com-

ponents: i) a plug-and-play sub-model to pre-process the encrypted CSIs, and ii) a commonly adopted HGR neural networks (e.g., Widar3 [10]). As shown in Figure 10, these two components are denoted by  $\mathcal{F}$  and  $\mathcal{R}$ , respectively. The output of this HGR pipeline is represented as  $z = \mathcal{R} \circ \mathcal{F}([\hat{\mathcal{H}}], \phi)$  where  $\phi$  represents the *key* generated by hashing the encryption matrix  $\Psi$  that has produced  $\hat{\mathcal{H}}$ . Consequently, instead of distributing  $\Psi$ , Alice needs only to securely share the key  $\phi$  with Bobs, and  $\phi$  is only several hundreds of bits at most given a normal cryptographic hash function (e.g., SHA-512 [48]). The sub-model  $\mathcal{F}$  to pre-process the encrypted CSIs is constructed and trained to adapt to encrypted CSIs produced by different  $\Psi$ 's; it outputs *surrogate CSIs*  $\check{\mathcal{H}}$  to properly drive the HGR neural network  $\mathcal{R}$  for classification. It is worth noting that  $\mathcal{F}$  does not perform  $\Psi$ -related matrix operation; otherwise it would have to bear a high complexity in both model parameters and training. This is possible because Bob<sup>S</sup> only demands the feature map generated by  $\mathcal{R}$  (given an input  $\check{\mathcal{H}}$ ) is well-aligned with the decision boundaries of its classifier; this is much easier than the symbol decoding by Bob<sup>C</sup> to be completed only within a very short period of Wi-Fi signals (i.e., a few readings of  $[\hat{\mathcal{H}}_m]$  for a given  $m$ ).

*Keyed Dynamic Neural Network.* To accommodate the CSIs encrypted with distinct encryption matrix  $\Psi$ , a naive solution is to train multiple versions of (static) neural networks  $[\mathcal{F}_1, \mathcal{F}_2, \dots]$ , according to different keys and CSIs produced by  $\Psi$ 's, and to switch to the corresponding version when processing certain input. However, this naive solution introduces large overhead in terms of storage and training time. Therefore, we borrow the idea from *dynamic neural networks* [49] that uses a small set of  $V$  parallel neural networks, each controlled by a gate, to form the sub-model  $\mathcal{F}$ . When in action, the controllable gates may allow  $\mathcal{F}$  to have up to  $2^V$  different structures, hence dynamically adapting  $\mathcal{F}$  to suit a particularly encrypted CSI input. In order to speed up the training, we deliberately add the key  $\phi$ ; it delivers extra information to control the gates.

Figure 10 illustrates our keyed dynamic neural network,

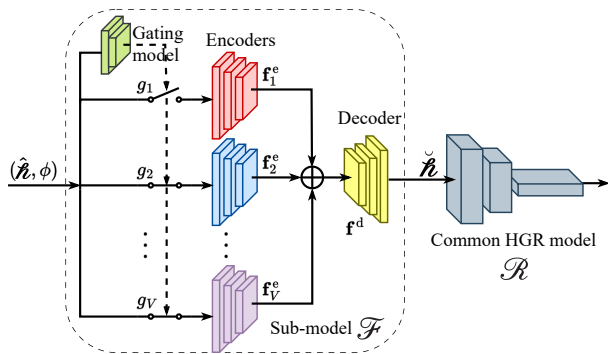


Figure 10: The “one-fits-all” HGR pipeline for MIMOCrypt; it involves a dynamically adaptable pre-processing sub-model  $\mathcal{F}$  and a common HGR model  $\mathcal{R}$ .

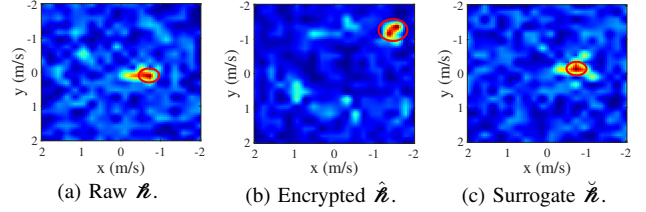


Figure 11: Feature maps of body-coordinate velocity profile (BVP) for Widar3 under different CSI inputs: (a) raw  $\hat{\mathcal{H}}$ , (b) encrypted  $\hat{\mathcal{H}}$ , and (c) surrogate  $\check{\mathcal{H}}$ .

where  $V$  encoders  $f_i^e$  are controlled by a gating model  $g$  to obtain adaptability and only one decoder  $f^d$  is used to generate the surrogate CSIs  $\check{\mathcal{H}}$ . Consequently, the sub-model  $\mathcal{F}$  can be represented as  $f^d \circ (\sum_{i=1}^V g_i \circ f_i^e)(\hat{\mathcal{H}}, \phi)$  where  $g_i \in \{0, 1\}$  is the binary output of  $g$  for controlling the activation of  $i$ -th encoder function  $f_i^e$ . We refer to Section 5 for detailed parameter settings for  $\mathcal{F}$ . During the training phase, we fix the weights for the pre-trained HGR model  $\mathcal{R}$  and only update the weights of  $\mathcal{F}$  via the gradient initiated by the cross-entropy loss function:

$$\min_{\mathcal{F}} - \frac{1}{|S|} \sum_{j \in S} \sum_{c \in C} y_{j,c} \log \left( [\mathcal{R} \circ \mathcal{F}(\hat{\mathcal{H}}, \phi)]_c \right) \quad (12)$$

where  $S$  and  $C$  are the set of training samples and classes, respectively. A trained  $\mathcal{F}$ , when facing a specific input pair  $(\hat{\mathcal{H}}, \phi)$ , shall be able to dynamically adapted to it via the combinatorial structure activated by  $g$  and hence to produce the correct surrogate CSIs  $\check{\mathcal{H}}$ . In Figure 11, we plot the feature maps generated by the Widar3 HGR model [10], given different CSI inputs: apparently, while the encrypted CSIs lead to very different feature maps from that of raw CSIs, surrogate CSIs may almost perfectly reproduce the feature maps of raw CSIs.

#### 4.6. Putting All Together

According to the illustration of Figure 1, a trusted party Alice controls Wi-Fi APs of an indoor space where privacy sensitivity is high. It applies encryption matrix  $\Psi$  to encrypt the channels (hence CSIs), so that any malicious eavesdroppers (Eves) obtaining the encrypted CSIs  $\hat{\mathcal{H}}$  cannot leverage them to infer hand gestures of a nearby victim, as proven in Section 4.3. In the meantime, the Wi-Fi network should also support legitimate users (Bobs) separated into two groups: Bob<sup>C</sup> and Bob<sup>S</sup> respectively use communication and sensing services. Upon Bobs’ registration with Alice, they become eligible to obtain the information about the encryption matrix  $\Psi$  (either direct or indirect as  $\phi$ ) from Alice for decrypting  $\hat{\mathcal{H}}$ . Since the MIMO encryption may still affect the performance of Bobs even after decryption, Alice optimizes  $\Psi$ 's (see Section 4.4), leveraging a novel sensing metric defined in Section 4.1, so as to strike a good balance between thwarting Eves and protecting Bobs. While

a key needs to be  $\Psi$  itself for Bob<sup>C</sup>, Bob<sup>S</sup> may enjoy a substantially improved efficiency with a hashed  $\Psi$  of only several hundreds of bits, as explained in Section 4.5.

## 5. IMPLEMENTATION

*Hardware.* We utilize the widely-adopted SDR platform WARP v3 [21] to build our MIMOCrypt prototype shown in Figure 12a. MIMOCrypt operates at 2.4 GHz with 20 MHz bandwidth, and AP (Alice) transmits packets at a default rate of 1,000 packets per second according to Widar3 [10] and WiSee [25]. Whereas we let Bob and Eve directly take the basic version of WARP node with 2 antennas, Alice is equipped with 8 antennas by leveraging FMC module Mango FMC-RF-2X245 [50] to extend the number of antennas in a single WARP node to 4 and then synchronizing two independent nodes via the clock module CM-MMCX [51]. All WARP nodes are connected to a PC server supported by an Intel Core i7-12700H CPU, 32GB RAM, and a GeForce RTX 3070Ti graphics card via a 1 GHz Ethernet switch, where the software of MIMOCrypt (described in the following) operates.

*Software.* We implement the software framework of MIMOCrypt in low level C language and Python 3.7 running on the PC server, with the neural models built upon PyTorch 1.11.0. As shown in Figure 10, we utilize Widar3 and WiSee as the common HGR models; they respectively depend on the body-coordinate velocity profile (BVP) and Doppler frequency shift (DFS) features. For our sensing sub-model  $\mathcal{F}$ , its gating model  $g$  uses a standard residual block [52] followed by 4 full-connection layers, with  $V = 8$  for our current design. Each of the 8 encoders consists of 4 consecutive convolutional layers, with a kernel size 3, stride 1, padding size 1, and their output channels being 32, 64, 64 and 128, respectively. For the decoder, 5 consecutive transposed convolutional layers constructed by ConvTranspose2d [53] are utilized, their kernel size is set to 3, as well as stridden to 1 (but 2 for the fourth layer), and the output channels of these layers are set to 64, 32, 32, 16 and 16, respectively. Finally, the output of each layer is followed by an activation function ReLU [54] and a normalization operator of BatchNorm2d [55]. During the training phase, all weights of  $\mathcal{F}$  are initialized by the Xavier uniform initializer [56],

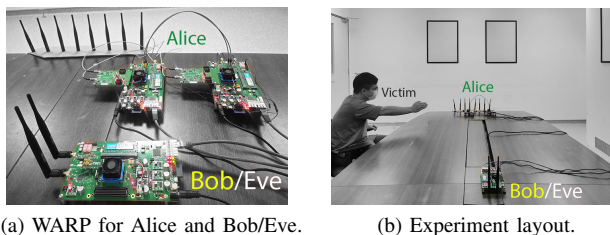


Figure 12: MIMOCrypt implementation: (a) WARP configurations and (b) experiment layout in an office area.

the random parameter dropout ratio is set to 0.5, and the batch size is 128. Meanwhile, RMSprop optimizer [57] is utilized to update parameters, with a learning rate is of 0.001. Upon inference, we deploy the keyed dynamic neural network (introduced in Section 4.5) in every Bob, but only the common HGR model on Eve.

## 6. EVALUATIONS

In this section, we first present the overall performance of MIMOCrypt in thwarting Eve, protecting legitimate sensing of Bob<sup>S</sup> and communication of Bob<sup>C</sup>. Then the impact of various parameter settings on our prototype is evaluated.

### 6.1. Experiment Setup

We recruit 6 volunteers (3 females and 3 males) as victims for participating in data collection. We first ask them to watch the example video for standardizing their gesture-performing behaviors. Then each victim performs eight common gestures (i.e., push-pull, clap, slide, tap, pinch-spread, drawing a circle, square, and zigzag) in a large meeting room with an area of about 32 m<sup>2</sup> as shown in Figure 12b. To ease the exposition, these gestures are abbreviated as PP, CL, SL, TA, PS, DC, DS, and DZ respectively. Given the passive nature of Wi-Fi sensing (see Section 2.2), we may leverage only one WARP node to emulate a multi-user scenario with several Bobs and Eves, by separately conducting either legitimate sensing or eavesdropping on the hand gestures of one target/victim. Of course, this does not emulate multi-Eve collusion cases, but such cases have been either forbidden or proven ineffective in Sections 2.2 and 4.3. We collect two datasets spanning totally 42.6 hours, corresponding to without/with enabling MIMOCrypt’s MIMO encryption: Data-1 contains 25920 samples (8 gestures  $\times$  540 instances  $\times$  6 objects) while Data-2 owns 8640 samples (8 gestures  $\times$  180 instances  $\times$  6 objects). The data collection process has strictly followed the standard procedures required by our IRB.

For adapting Widar3 and WiSee to our environment while optimizing parameters of  $\mathcal{F}$ , we leverage two-thirds of samples in Data-1 to retrain them and the remaining part for testing gesture recognition result. Moreover, MIMOCrypt employs two common metrics, namely accuracy and bit error ratio (BER), to quantify sensing and communication performance, where  $\text{accuracy} = \frac{N^{\text{cor}}}{N^{\text{all}}}$  measures the ratio of correctly recognized gestures, with  $N^{\text{cor}}$  and  $N^{\text{all}}$  respectively denoting the number of correctly recognized and of all gestures, and  $\text{BER} = \frac{N^{\text{err}}}{N^{\text{all}}}$  indicates the ratio of incorrectly decoded bits, with  $N^{\text{err}}$  and  $N^{\text{all}}$  being the number of error bits and of totally transmitted bits, respectively.

### 6.2. MIMOCrypt Performance

**6.2.1. Thwarting Eve.** To evaluate the performance of MIMOCrypt on thwarting malicious eavesdropping via

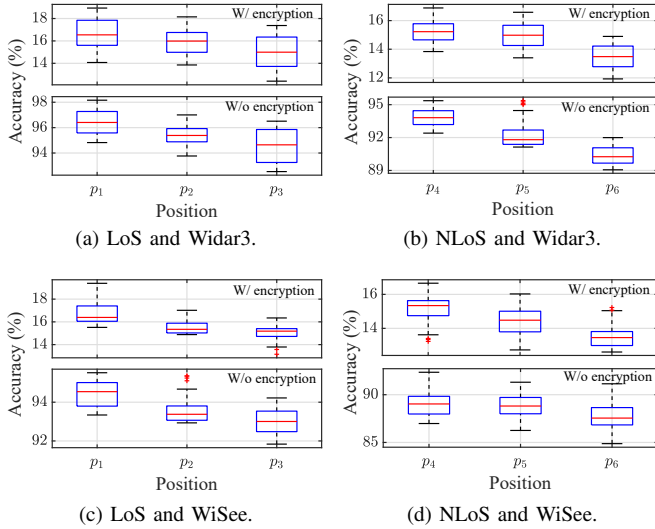


Figure 13: Eve's eavesdropping performance evaluated by Widar3 under (a) LoS and (b) NLoS, when turning on/off spatial-temporal encryption; the results under similar settings for WiSee are further shown in (c) and (d).

*spatial-temporal encryption*, we place Eve at six positions: the first three (i.e.,  $p_1$ ,  $p_2$ , and  $p_3$ ) having LoS path with Alice, at a distance of 1.5 m, 3 m and 4.5 m respectively; the others ( $p_4$ ,  $p_5$ , and  $p_6$ ) are co-located with previous ones but changed to NLoS type by adding obstacles in-between. The victim performs different hand gestures at 0.5 m from Alice. As shown in Figure 13a, with encryption, Eve's eavesdropping (HGR) accuracy on average is less than 16% in three LoS positions: compared with eavesdropping without encryption, MIMOCrypt has successfully reduced Eve's HGR accuracy by about 80%. A similar trend for the NLoS setting is further demonstrated by Figure 13b, while both results also confirm that Eve's eavesdropping performance can also be worsen by either a longer distance or certain obstacles, consistent with our study in Section 4.1. Finally, we leverage another well-known HGR model WiSee (also adopted by PhyCloak [15]) to reconfirm the excellent performance of MIMOCrypt for thwarting Eve in Figure 13c and 13d. The results clearly indicate that the encryption

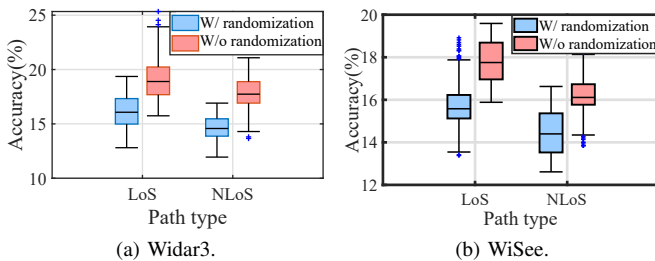


Figure 14: Eve's gesture recognition accuracy when using (a) Widar3 and (b) WiSee respectively, with/without enabling the temporal randomization.

matrix  $\Psi$ , endowed with diversified choices from full space (as described in Section 4.3), can effectively encrypt a wide range of channels to thwart Eve's attacks.

We also evaluate MIMOCrypt's temporal randomization performance against Eve; the results are reported in Figure 14. Essentially, temporal randomization further reduces Eve's eavesdropping accuracy by 4.87% for Widar3 and 6.01% for WiSee; it also lessens the accuracy difference between LoS and NLoS to only 0.32%. The effectiveness of temporal randomization can be attributed to the common HGR model often pre-trained based on fixed and regular input (CSI) sample intervals.

**6.2.2. Protecting Bob<sup>S</sup>.** Apart from effectively thwarting Eve, MIMOCrypt also needs to retain the sensing ability of Bob<sup>S</sup>. Therefore, we hereby verify this performance aspect of MIMOCrypt by comparing the Bob<sup>S</sup>'s HGR accuracy at the same six positions taken by Eve earlier to ensure a fair comparison. The common HGR models adopted are again Widar3 and WiSee, but we consider two settings: i) non-encrypted CSIs fed to these models and ii) encrypted CSIs fed to  $\mathcal{F}$  before using these models as classifiers.

Figures 15a and 15b present the average accuracy of HGR by Widar3 and WiSee, respectively. Apparently, the HGR accuracy for Bob<sup>S</sup> only drops slightly when the encryption function is turned on, proving MIMOCrypt's efficacy on this performance aspect. Among all gestures, drawing circle (DC) and square (DS) have relatively lower recognition accuracy since differentiating them is indeed a challenge. Also, the average accuracy 90.62% of WiSee is lower than Widar3's 92.74%, suggesting that the BVP feature employed by Widar3 may be more robust to en-

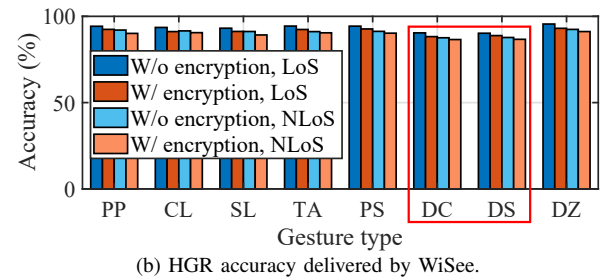
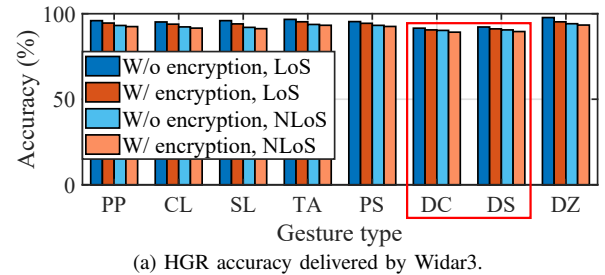


Figure 15: HGR accuracy of Bob<sup>S</sup> given i) non-encrypted CSIs and ii) encrypted ones filtered by  $\mathcal{F}$  before Widar3 (a) and WiSee (b), under both LoS and NLoS settings.

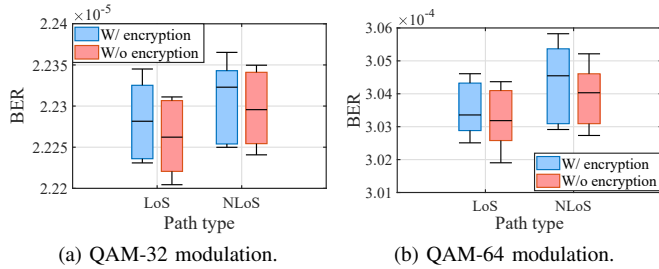


Figure 16: BERs of payload data modulated by QAM-32 (a) and QAM-64 (b), respectively, under the two cases of enabling and disabling MIMOCrypt encryption.

environment interference than the DFS of WiSee. Therefore, extracting environment-robust (cross-domain) features to construct HGR models can make it more practical.

**6.2.3. Protecting Bob<sup>C</sup>.** In this section, we evaluate the communication performance of MIMOCrypt in protecting Bob<sup>C</sup>, using BER of payload as the metric. We randomly choose 28 positions for Bob<sup>C</sup> to measure its BER. At each position, we let Alice communicate with Bob<sup>C</sup> for 30 minutes, using two common modulations (QAM-32 and QAM-64) for payload, and Bob<sup>S</sup> also performs HGR from time to time.<sup>4</sup> The boxplots in Figure 16 demonstrate that MIMOCrypt only affects the communication performance to a negligible extent: the median BER increases only in the digit of  $10^{-6}$ , and the BER variances are also increased at the same order, regardless of whether it is LoS or NLoS setting and what modulation scheme is adopted. MIMOCrypt achieves this excellent performance (for both Bob<sup>C</sup> and Bob<sup>S</sup>) thanks to our multi-objective optimization framework in Section 4.4 that successfully reaches the best tradeoff among conflicting objectives; this is in stark contrast to existing proposals that simply evaluate special cases to “prove” their channel scrambling barely affecting communications [15], [18].

### 6.3. Impact of Parameter Settings

We hereby study the impact of several system parameters on MIMOCrypt.

**6.3.1. Encryption Matrix Optimization.** According to Section 4.4, we leverage a multi-objective optimization framework to identify the optimal  $\Psi$ 's realizing the best tradeoffs among the performances of Eve, Bob<sup>S</sup> and Bob<sup>C</sup>. We randomly generate five hundred  $\Psi$ 's, and use them as the initial solution. We further obtain the same number of optimized  $\Psi$ 's. The results in Figure 17 clearly demonstrate that, compared with random  $\Psi$ 's, the optimized ones have much better performances in terms of worsening the sensing

4. These two users share the same device in our experiments, yet they can be either separated or co-located in reality.

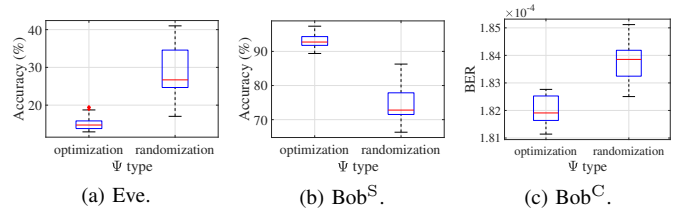


Figure 17: MIMOCrypt’s performance for (a) eavesdropping, (b) legitimate sensing, and (c) data communication under optimized or randomized encryption matrices.

accuracy of Eve, improving that of Bob<sup>S</sup>, and reducing the BER for Bob<sup>C</sup>. This firmly indicates that MIMOCrypt can successfully identify the best tradeoffs on the Pareto optimal frontier of the multi-objective optimization.

**6.3.2. Sub-model for Bob<sup>S</sup>'s Sensing.** To verify the effectiveness of our design in Section 4.5, we calculate the cosine similarity of the feature maps respectively induced by encrypted, decrypted, and surrogate CSIs with those induced by raw CSIs. For a fairness comparison, we use the same Data-1 (introduced in Section 6.1) to obtain the results. As shown in Figure 18a, the average correlation between surrogate and raw feature maps is around 90%, only 1.5% lower than that of the decrypted ones, clearly explaining why our sub-model can still perform accurate HGR shown in Figure 15.

We also study how the parameter  $V$  of the encoders quantity affects the sub-model. We adjust  $V$  from 2 to 16, and then plot the corresponding feature map correlations in Figure 18b. Apparently, the performance saturates after

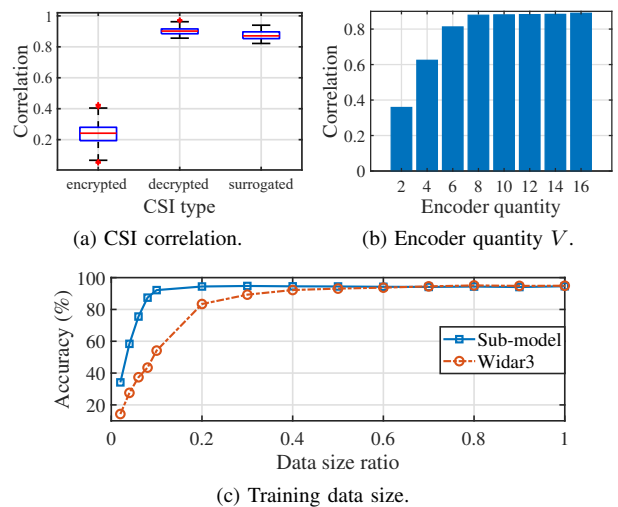


Figure 18: The power of surrogating: (a) correlations between three types of feature maps (encrypted, decrypted and surrogated and the the raw ones), (b) the impact of encoder quantity  $V$ , and (c) the impact of training data size on sub-model performance.

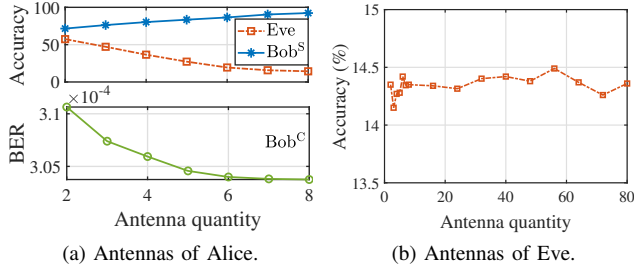


Figure 19: Antenna matters? (a) MIMOCrypt’s improved performance when increasing antenna quantity for Alice, and (b) increasing that quantity for Eve fails to work.

$V = 8$ , so we set the default  $V$  as 8 in our prototype. These results also corroborate our statement in Section 4.5 that, instead of a naive solution using a large number of static models, our sub-model only needs a small value of  $V$ , even for a large quantity of  $\Psi$ ’s. Moreover, training data size determines whether our sub-model can fully understand feature structures. To study its impact, we train the sub-model with increasing fraction of data, and compare the resulting accuracy with that of the Widar3 HGR model (during pre-training phase) in Figure 18c. Apparently, training our sub-model converges much faster (at least five times) than pre-training Widar3.

**6.3.3. Antenna Quantity.** For Alice, a large number of antennas allows it to improve both the diversity in  $\Psi$  (thwarting Eve) and the signal power distribution (protecting Bobs). Figure 19a presents MIMOCrypt’s improved performance (on both sides) when equipping Alice with an increasing number of antennas. Moreover, though we have argued in Section 2.2 that Eves often cannot have too many physical antennas, they may leverage virtual antennas (by changing positions at different times) [58] to gain higher diversity. Fortunately, the results in Figure 19b evidently confirm that, with up to 80 virtual antennas, Eve has no chance to crack  $\Psi$ ’s and thus to improve its HGR accuracy, even with higher diversity in both time and space, as proven in Section 4.3.

**6.3.4. Cost Reduction in Legitimate Sensing.** For Bob<sup>S</sup>, MIMOCrypt achieves cost reduction in two aspects: i) it cuts the transmission volume by employing a much shorter decryption key to replace  $\Psi$  thanks to the lower signal granularity demanded by gesture sensing, and ii) it substantially lessens the computation time cost by directly leveraging encrypted CSIs for gesture recognition, avoiding additional  $\Psi$ -related matrix operations. We hereby conduct a simple case study based on our experiment parameters to concretely demonstrate these two aspects.

On one hand, given the settings of Alice’s 8 antenna transmitting 1,500 packets (for a 1.5-second gesture) to Bob<sup>S</sup>, the encryption matrix  $\Psi$  contains  $8 \times 1500$  complex numbers (roughly 4 bytes each) and the total data volume is 48,000 bytes, since  $\Psi$  covers spatial-temporal dimensions

as introduced in Section 4.2. However, MIMOCrypt only relies on a decryption key  $\phi$  to activate specific encoders for processing the encrypted CSIs, so the transmission volume is reduced to the 2048-bit decryption key, less than 0.54% of the original volume. Although either  $\Psi$  or  $\phi$  needs only to be updated periodically (e.g., every several weeks or even months) as explained in Sections 4.3, 4.4, and 4.5, such a reduction is still significant.

On the other hand, each  $\Psi$ -related decryption (matrix) operation needs an extra 0.83 ms as indicated in Section 3.3, so the extra time cost for a 1.5-second gesture is reduced from  $1500 \times 0.83 = 1245$  ms (given the packet rate of 1,000 packets per second) to zero; here only the extra time cost matters because the average inference times of the normal HGR models with and without the sub-model  $\mathcal{F}$  are very close to each other. To sum up, our plug-and-play sub-model can provide evident cost reduction in both transmission volume and computation time.

## 7. LIMITATIONS AND DISCUSSIONS

*New User Registration.* We have so far implicitly assumed that Bobs have registered to Alice before MIMOCrypt activating its encryption, but what about newly joining Bobs? After activating MIMO encryption, unregistered Bobs are treated as the Eves, and hence face difficulty in further registration (albeit still possible as a Bob enjoy non-zero communication throughput under encryption). To address this issue under Wi-Fi standard, the Alice may sporadically broadcast Wi-Fi’s beacon frames without encryption, hence providing opportunity for newly arriving Bobs to register. Since the beacon frames are relatively short [59] and Eves are not interested in registration for the sake of its stealthiness (see Section 2.2), accommodating newly joining Bobs should be readily solvable for MIMOCrypt.

*Analysis on Physical Encryption.* As discussed in Section 4.3, MIMOCrypt excels in applying digitally controlled MIMO beamformers to physically encrypt physical plaintext (e.g., hand gestures), as opposed to existing (seemingly similar) techniques of *orthogonal blinding* [34]–[36] that only physically obfuscate digital plaintext. The resulting benefit is twofold: full-scale KPA is too obvious due to its physical presence and hence forbidden on one hand (see Section 2.2), while on the other hand, side-channel KPA barely affects the encryption strength as the conditional entropy of physical ciphertext is evaluated in statistical sense (instead of the combinatorial sense for digital ciphertext), as the entropy is now closely related to SNR [41], [42]. Applying physical encryption based on complex multiplication (as opposed to the permutation used for digital encryption) also allows for further optimization on the choice of keys, which is a concept absent from conventional cryptography. This makes us believe that we may extend such encryption schemes to secure digital plaintext too. Nonetheless, it is unclear how to perform formal security analysis on physical encryption: to

the best of our knowledge, convention attacks to encryption schemes, such as brute-force attack, known-plaintext attack, and differential cryptanalysis, may not be readily migrated to this new case. Consequently, we would leave this problem open for future exploration.

## 8. CONCLUSION

In this paper, we have designed and implemented MIMOCrypt as a MIMO-driven privacy-preserving system for supporting multi-user Wi-Fi sensing and communication applications. In particular, we have proposed a source-defined channel encryption to thwart stealthy Wi-Fi eavesdropping attack and seriously analyzed its security. To strike an adequate balance between thwarting attacks and preserving legitimate services, we have explored a multi-objective optimization framework to guide the channel encryption design. Finally, we have innovated in a keyed dynamic neural network to produce surrogate CSIs for legitimate sensing users and hence to reduce the key distribution load for them. Our extensive experiments with a WARP-based MIMOCrypt prototype have evidently demonstrated the efficacy of MIMOCrypt in securing sensing and protecting entitled abilities of legitimate users.

## Acknowledgement

We are grateful to anonymous reviewers for their constructive suggestions. This research is supported by National Research Foundation, Singapore and Infocomm Media Development Authority under its Future Communications Research & Development Programme grant FCP-NTU-RG-2022-015, as well as MoE Tier 1 grant RG16/22. Zhe Chen is the corresponding author.

## References

- [1] F. Adib and D. Katabi, "See through Walls with WiFi!" in *Proc. of the 27th ACM SIGCOMM*, 2013, pp. 75–86.
- [2] G. Wang, Y. Zou, Z. Zhou, K. Wu, and L. M. Ni, "We Can Hear You with Wi-Fi!" in *Proc. of the 20th ACM MobiCom*, 2014, pp. 593–604.
- [3] C. Zhang, F. Li, J. Luo, and Y. He, "iLocScan: Harnessing Multipath for Simultaneous Indoor Source Localization and Space Scanning," in *Proc. of the 12th ACM SenSys*, 2014, p. 91–104.
- [4] K. Joshi, D. Bharadia, M. Kotaru, and S. Katti, "WiDeo: Fine-grained Device-free Motion Tracing using RF Backscatter," in *Proc. of the 12nd USENIX NSDI*, 2015, pp. 189–204.
- [5] J. Liu, Y. Wang, Y. Chen, J. Yang, X. Chen, and J. Cheng, "Tracking Vital Signs During Sleep Leveraging Off-the-Shelf WiFi," in *Proc. of the 16th ACM MobiHoc*, 2015, p. 267–276.
- [6] K. Ali, A. X. Liu, W. Wang, and M. Shahzad, "Keystroke Recognition Using WiFi Signals," in *Proc. of the 21st ACM MobiCom*, 2015, pp. 90–102.
- [7] J. Wang, H. Jiang, J. Xiong, K. Jamieson, X. Chen, D. Fang, and B. Xie, "LiFS: Low Human-Effort, Device-Free Localization with Fine-Grained Subcarrier Information," in *Proc. of the 22nd ACM MobiCom*, 2016, pp. 243–256.
- [8] X. Wang, K. Niu, J. Xiong, B. Qian, Z. Yao, T. Lou, and D. Zhang, "Placement Matters: Understanding the Effects of Device Placement for WiFi Sensing," *Proc. ACM Interact. Mob. Wearable Ubiquitous Technol.*, vol. 6, no. 1, pp. 32:1–25, 2022.
- [9] D. Halperin, W. Hu, A. Sheth, and D. Wetherall, "Tool Release: Gathering 802.11n Traces with Channel State Information," *ACM SIGCOMM Comput. Commun. Rev.*, vol. 41, no. 1, p. 53, 2011.
- [10] Y. Zheng, Y. Zhang, K. Qian, G. Zhang, Y. Liu, C. Wu, and Z. Yang, "Zero-Effort Cross-Domain Gesture Recognition with Wi-Fi," in *Proc. of the 17th ACM MobiSys*, 2019, pp. 313–325.
- [11] S. Zhang, T. Zheng, Z. Chen, and J. Luo, "Can We Obtain Fine-grained Heartbeat Waveform via Contact-free RF-sensing?" in *Proc. of the 41st IEEE INFOCOM*, 2022, pp. 1759–1768.
- [12] S. Fang, I. Markwood, Y. Liu, S. Zhao, Z. Lu, and H. Zhu, "No Training Hurdles: Fast Training-agnostic Attacks to Infer Your Typing," in *Proc. of the 25th ACM CCS*, 2018, pp. 1747–1760.
- [13] E. Yang, Q. He, and S. Fang, "WINK: Wireless Inference of Numerical Keystrokes via Zero-Training Spatiotemporal Analysis," in *Proc. of the 29th ACM CCS*, 2022, pp. 3033–3047.
- [14] J. Hu, H. Wang, T. Zheng, J. Hu, Z. Chen, H. Jiang, and J. Luo, "Password-Stealing without Hacking: Wi-Fi Enabled Practical Keystroke Eavesdropping," in *Proc. of the 30th ACM CCS*, 2023, p. 1–14.
- [15] Y. Qiao, O. Zhang, W. Zhou, K. Srinivasan, and A. Arora, "PhyCloak: Obfuscating Sensing from Communication Signals," in *Proc. of the 13rd USENIX NSDI*, 2016, pp. 685–699.
- [16] M. Li, Y. Meng, J. Liu, H. Zhu, X. Liang, Y. Liu, and N. Ruan, "When CSI Meets Public WiFi: Inferring Your Mobile Phone Password with WiFi Signals," in *Proc. of the 23rd ACM CCS*, 2016, p. 1068–1079.
- [17] Y. Zhu, Z. Xiao, Y. Chen, Z. Li, M. Liu, B. Y. Zhao, and H. Zheng, "Et Tu Alexa? When Commodity WiFi Devices Turn into Adversarial Motion Sensors," in *Proc. of the 27th ISOC NDSS*, 2020, pp. 1–15.
- [18] P. Staat, S. Mulzer, S. Roth, V. Moonsamy, M. Heinrichs, R. Kronberger, A. Sezgin, and C. Paar, "IRShield: A Countermeasure Against Adversarial Physical-Layer Wireless Sensing," in *Proc. of the 43rd IEEE S&P*, 2022, pp. 1526–1526.
- [19] J. Hu, T. Zheng, Z. Chen, H. Wang, and J. Luo, "MUSE-Fi: Contactless Multi-person Sensing Exploiting Near-field Wi-Fi Channel Variation," in *Proc. of the 29th ACM MobiCom*, 2023, pp. 1–15.
- [20] Z. Chen, T. Zheng, C. Cai, and J. Luo, "MoVi-Fi: Motion-robust Vital Signs Waveform Recovery via Deep Interpreted RF Sensing," in *Proc. of the 27th ACM MobiCom*, 2021, p. 392–405.
- [21] Mango Communications, "WARP v3 Kit," <http://mangocomm.com/products/kits/warp-v3-kit/>, 2022, online; accessed 18 August 2022.
- [22] B. A. L. S. and S. S., "Channel Estimation Techniques with Long Training Sequence for IEEE802.11A," in *Proc. of IEEE SPCOM*, 2004, pp. 136–139.
- [23] Z. Yang and J. Kimmo, "The Death and Rebirth of Privacy-Preserving WiFi Fingerprint Localization with Paillier Encryption," in *Proc. of the 37th IEEE INFOCOM*, 2018, pp. 1223–1231.
- [24] Y. Ma, G. Zhou, and S. Wang, "WiFi Sensing with Channel State Information: A Survey," *ACM Comput. Surv.*, vol. 52, no. 3, pp. 46:1–36, 2019.
- [25] Q. Pu, S. Gupta, S. Gollakota, and S. Patel, "Whole-Home Gesture Recognition Using Wireless Signals," in *Proc. of the 19th ACM MobiCom*, 2013, p. 27–38.
- [26] C. Wang, X. Zheng, Y. Chen, and J. Yang, "Locating Rogue Access Point Using Fine-Grained Channel Information," *IEEE Trans. on Mobile Computing*, vol. 16, no. 9, pp. 2560–2573, 2017.

- [27] Y. Yao, Y. Li, X. Liu, Z. Chi, W. Wang, T. Xie, and T. Zhu, "Aegis: An Interference-Negligible RF Sensing Shield," in *Proc. of the 37th IEEE INFOCOM*, 2018, pp. 1718–1726.
- [28] K. Qian, C. Wu, Z. Yang, Z. Zhou, X. Wang, and Y. Liu, "Enabling Phased Array Signal Processing for Mobile WiFi Devices," *IEEE Transactions on Mobile Computing*, vol. 17, no. 8, pp. 1820–1833, 2018.
- [29] D. Bharadia, E. McMillin, and S. Katti, "Full Duplex Radios," in *Proc. of the 27th ACM SIGCOMM*, 2013, pp. 375–386.
- [30] T. Cui, M. Qi, X. Wan, J. Zhao, and Q. Cheng, "Coding Metamaterials, Digital Metamaterials and Programmable Metamaterials," *Light: Science & Applications*, vol. 3, no. e218, 2014.
- [31] X. Jiao, M. Mehari, W. Liu, M. Aslam, and I. Moerman, "Openwifi CSI Fuzzer for Authorized Sensing and Covert Channels," in *Proc. of the 14th ACM WiSec (Demo)*, 2021, pp. 377–379.
- [32] S. Heron, "Advanced Encryption Standard (AES)," *Elsevier Network Security*, pp. 8–12, 2009.
- [33] A. Van Zelst and T. C. Schenk, "Implementation of a MIMO OFDM-based Wireless LAN System," *IEEE Transactions on Signal Processing*, pp. 483–494, 2004.
- [34] N. Anand, S.-J. Lee, and E. W. Knightly, "STROBE: Actively Securing Wireless Communications using Zero-Forcing Beamforming," in *Proc. of the 31st IEEE INFOCOM*, 2012, pp. 720–728.
- [35] M. Schulz, A. Loch, and M. Hollick, "Practical Known-Plaintext Attacks against Physical Layer Security in Wireless MIMO Systems," in *Proc. of the 21st ISOC NDSS*, 2014, pp. 1–13.
- [36] Y. Pan, Y. Zheng, and M. Li, "ROBin: Known-Plaintext Attack Resistant Orthogonal Blinding via Channel Randomization," in *Proc. of the 39th IEEE INFOCOM*, 2020, pp. 1927–1936.
- [37] S. Sur, I. Pefkianakis, X. Zhang, and K.-H. Kim, "Practical MU-MIMO User Selection on 802.11ac Commodity Networks," in *Proc. of the 22nd ACM MobiCom*, 2016, p. 122–134.
- [38] S. Ding, Z. Chen, T. Zheng, and J. Luo, "RF-Net: A Unified Meta-Learning Framework for RF-Enabled One-Shot Human Activity Recognition," in *Proc. of the 18th ACM SenSys*, 2020, pp. 517–530.
- [39] W. Du, J. Deng, Y. S. Han, P. K. Varshney, J. Katz, and A. Khalili, "A Pairwise Key Predistribution Scheme for Wireless Sensor Networks," *ACM Transactions on Information and System Security*, vol. 8, no. 2, p. 228–258, 2005.
- [40] D. Han, A. Li, J. Li, Y. Zhang, T. Li, and Y. Zhang, "DroneKey: A Drone-Aided Group-Key Generation Scheme for Large-Scale IoT Networks," in *Proc. of the 28th ACM CCS*, 2021, p. 1306–1319.
- [41] D. Guo, S. Shamaï (Shitz), and S. Verdú, "The Interplay Between Information and Estimation Measures," *Foundations and Trends® in Signal Processing*, no. 4, pp. 243–429, 2013.
- [42] J. Polcari, "An Informative Interpretation of Decision Theory: The Information Theoretic Basis for Signal-to-Noise Ratio and Log Likelihood Ratio," *IEEE Access*, vol. 1, pp. 509–522, 2013.
- [43] A. J. Menezes, P. C. Van Oorschot, and S. A. Vanstone, *Handbook of Applied Cryptography*. CRC press, 2018.
- [44] W. Li and N. C. Beaulieu, "Effects of channel-estimation errors on receiver selection-combining schemes for Alamouti MIMO systems with BPSK," *IEEE Transactions on Communications*, pp. 169–178, 2006.
- [45] IEEE, "IEEE Standard for Information Technology–Telecommunications and Information Exchange between Systems Local and Metropolitan Area Networks–Specific Requirements Part 11: Wireless LAN Medium Access Control (MAC) and Physical Layer (PHY) Specifications Amendment 1: Enhancements for High-Efficiency WLAN," *IEEE Std 802.11ax-2021 (Amendment to IEEE Std 802.11-2020)*, pp. 1–767, 2021.
- [46] S. Boyd and L. Vandenberghe, *Convex Optimization*. Cambridge University Press, March 2004.
- [47] S. Boyd, N. Parikh, E. Chu, B. Peleato, J. Eckstein *et al.*, "Distributed Optimization and Statistical Learning via the Alternating Direction Method of Multipliers," *Foundations and Trends® in Machine Learning*, vol. 3, no. 1, pp. 1–122, 2011.
- [48] S. Gueron, S. Johnson, and J. Walker, "SHA-512/256," in *Proc. of the 8th IEEE ITNG*, 2011, pp. 354–358.
- [49] Y. Han, G. Huang, S. Song, L. Yang, H. Wang, and Y. Wang, "Dynamic Neural Networks: A Survey," *IEEE Transactions on Pattern Analysis and Machine Intelligence*, 2021.
- [50] Mango Communications, "FMC-RF-2X245: Dual-Radio FMC Module," <https://mangocomm.com/products/modules/fmc-rf-2x245/>, 2022, online; accessed 4 August 2022.
- [51] Mango Communication, "CM-MMCX: WARP v3 Clock Module with MMCX connectors," <https://www.mangocomm.com/products/modules/cm-mmcx/>, 2022, online; accessed 4 August 2022.
- [52] K. He, X. Zhang, S. Ren, and J. Sun, "Deep Residual Learning for Image Recognition," in *Proc. of the 26th IEEE CVPR*, 2016.
- [53] PyTorch, "ConvTranspose2d," <https://pytorch.org/docs/stable/generated/torch.nn.ConvTranspose2d.html>, 2022, online; accessed 4 August 2022.
- [54] Vinod Nair and Geoffrey E. Hinton, "Rectified Linear Units Improve Restricted Boltzmann Machines," in *Proc. of the 27th ICML*, 2010, pp. 807–814.
- [55] S. Ioffe and C. Szegedy, "Batch Normalization: Accelerating Deep Network Training by Reducing Internal Covariate Shift," in *Proc. of the 32nd ICML*, 2015, pp. 448–456.
- [56] X. Glorot and Y. Bengio, "Understanding the Difficulty of Training Deep Feedforward Neural Networks," in *Proc. of the 13th PMLR*, vol. 9, 2010, pp. 249–256.
- [57] PyTorch, "RMSprop," <https://pytorch.org/docs/stable/generated/torch.optim.RMSprop.html?highlight=rmsprop>, 2022, online; accessed 4 August 2022.
- [58] S. Kumar, S. Gil, D. Katabi, and D. Rus, "Accurate Indoor Localization with Zero Start-up Cost," in *Proc. of the 20th ACM MobiCom*, 2014, p. 483–494.
- [59] H. Lee, J. Kim, C. Joo, and S. Bahk, "BeaconRider: Opportunistic Sharing of Beacon Air-Time in Densely Deployed WLANs," in *Proc. of the 27th IEEE ICNP*, 2019, pp. 1–11.
- [60] D. Tse and P. Viswanath, *Fundamentals of Wireless Communication*. Cambridge University Press, 2005.
- [61] R. Xiao, J. Liu, J. Han, and K. Ren, "OneFi: One-Shot Recognition for Unseen Gesture via COTS WiFi," in *Proc. of the 19th ACM SenSys*, 2021, p. 206–219.
- [62] W. Wang, A. X. Liu, M. Shahzad, K. Ling, and S. Lu, "Understanding and Modeling of WiFi Signal Based Human Activity Recognition," in *Proc. of the 21st ACM MobiCom*, 2015, p. 65–76.
- [63] Z. Chen, T. Zheng, and J. Luo, "Octopus: A Practical and Versatile Wideband MIMO Sensing Platform," in *Proc. of the 27th ACM MobiCom*, 2021, pp. 601–614.
- [64] Z. Chen, T. Zheng, C. Hu, H. Cao, Y. Yang, H. Jiang, and J. Luo, "ISACoT: Integrating Sensing with Data Traffic for Ubiquitous IoT Devices," *IEEE Communications Magazine*, vol. 61, no. 5, pp. 98–104, 2023.
- [65] J. Shenoy, Z. Liu, B. Tao, Z. Kabelac, and D. Vasisht, "RF-Protect: Privacy against Device-free Human Tracking," in *Proc. of the 36th ACM SIGCOMM*, 2022, pp. 588–600.

## Appendix A. Extended Security Analysis

Given limited space for the main texts, we spare some detailed analysis to this appendix, focusing on issues not fully discussed in Sections 4.3 and 7, including whether certain side-channel may substantially reduce the entropy of the encryption to the extend of breaking it.

First of all, as MIMOCrypt applies a formal cryptographic encryption with a sequence of scrambling patterns and the sequence length as the key length, it is fundamentally different from the orthogonal blinding schemes appeared in [34], [36] in mainly two aspects. On one hand, as legitimate users (Bobs) can obtain a key for CSI decryption, the encryption keys can be chosen within a full space, rather than forced to stay in orthogonal to Bobs' channel for blinding Eves. On the other hand, as MIMOCrypt's encryption key often has a length of around or even over 1,000 scrambling patterns (as shown in Section 6.3.4) that get switched from one to another in millisecond scale, the numerical analysis of how entropy decays in time [36] does not apply anymore. In short, MIMOCrypt's physical encryption is much stronger than existing orthogonal blinding.

Second, one may wonder if a period of no activity may leak the information about MIMOCrypt's encryption key. In fact, such a period can be deemed as the static background already counted in Eqn. (5): as it is statistically independent of gestures, it does not matter if the CSIs are encrypted or not, and the related term in the denominator of Eqn. (5) simply takes the unencrypted form. Therefore, eavesdropping no-activity period does not concern the strength of MIMOCrypt's protection at all. Moreover, a no-activity period bears no function of "pilot signal" that leverages known information to probe unknown one (e.g., known LTS to probe the channel). As MIMOCrypt encrypts the channel, both the encryption key and the channel are unknown. As we have discussed in Sections 4.3 and 6.3.3, this situation makes adding observation diversity (either temporal by observing longer or spatial by adding antennas) totally fruitless. Note that channel conditions may still vary and become independent beyond coherence time [60], so no activity does not suggest static CSIs.

Third, there exists a major difference in the interpretation of *entropy* (commonly used for security analysis) between digital and physical plaintexts: whereas the former can be computed in absolute sense given the discrete distribution of digital symbols (e.g., entropy may become zero if the encryption key is exposed), the latter is characterized in relative sense against the noise [41] and hence get related to SNR, which may never become zero but can be maximized if the signal is scrambled to be under the noise floor. Consequently, unlike digital encryption (upon digital plaintext) for which exposing a few pairs of unencrypted and encrypted symbols can substantially decrease the entropy of encryption, the same exposure causes negligible loss

in (relative) entropy for physical encryption, because SNR is computed in statistical sense by averaging across many observations/samples. Therefore, as argued in Section 4.3, side-channel KPA most likely fails to break MIMOCrypt; as far as we understand, the only chance one may break MIMOCrypt is via a full-scale KPA to re-train the HGR model under encrypted CSIs, but this is forbidden by our attack model in Section 2.2.

Last but not least, we have omitted the analysis on the sub-model  $\mathcal{F}$  introduced in Section 4.5, for a slightly different reason as that explained in Section 7 for physical encryption. Although we suspect that hashing  $\Psi$  to produce  $\phi$  should not affect the encryption strength, our current proposal in Section 4.5 still requires  $\mathcal{F}$  to be distributed only to Bob<sup>S</sup>, albeit no apparent reason against also exposing  $\mathcal{F}$  to Eves (as the case for the common HGR models). In general, the security analysis on physically encrypted physical plaintext is somehow "interfered" by the existence of a deep learning model acting as a "translator" between physical plaintexts and their digital labels (or interpretations). Whereas the security issue of such models in terms of being tricked to generate wrong translations (a.k.a, adversarial examples) is well understood, whether one can breach a keyed model like our  $\mathcal{F}$  so as to obtained the encrypted translations remains a largely unexplored question.

## Appendix B. Extended Experiments

*The Impact of Packet Transmission Rate.* Packet transmission rate (PTR) can directly impose effects on signal density and hence sensing tasks, and it also affects how fast  $\Psi$  switches its scrambling patterns from one to the next. MIMOCrypt sets the default PTR to 1,000 packets per second referring to [10], [25], [61], to provide sufficient channel information density for gesture recognition. However, the LTS-based CSI estimation is designed for data communication services, not specifically for sensing. Therefore, PTR is determined by communication service-related parameter settings, such as Wi-Fi protocols and wireless channel states. Subsequently, we adjust PTR to the range from 100 to 1,500 pkt/s for fully evaluate MIMOCrypt under distinct communication environments. As depicted in Figure 20b, the legitimate sensing accuracy owns a slight improvement when the PTR (less than 0.4k) increases, and then stabilizes around 93.5% of Widar3 and 90.8% of WiSee. Moreover, thwarting eavesdropping in Figure 20a and protecting legitimate communication in Figure 20c keep a stable and satisfactory performance in the full PTR range. In general, these experiments lead to two conclusions: MIMOCrypt can be adequately compatible with distinct PTR value settings, thus PTR imposes negligible effect on our privacy-preserving mechanism for Wi-Fi sensing; the reason why malicious eavesdropping can be successfully obfuscated is driven by MIMOCrypt rather than signal granularity.

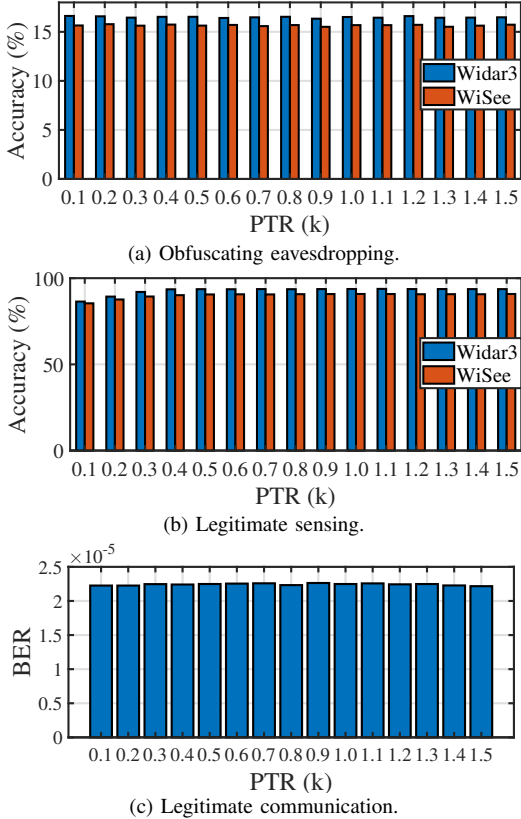


Figure 20: MIMOCrypt’s performance in (a) thwarting Eve, while (b) protecting Bob<sup>S</sup> and (c) Bob<sup>C</sup>, under distinct packet transmission rates.

*The Impact of Random Packet Interval.* MIMOCrypt adds temporal randomization to fixed packet transmission interval to achieve temporal randomization, which complements the spatial-temporal encryption for further obfuscating the correspondence between CSI features and gestures. In Section 6.2.1, we evaluate the effectiveness of temporal randomization as the randomized “jitter” ratio  $\beta_m$  falls within  $[-0.5, 0.5]$ . Since the  $\beta_m$ ’s value boundary  $\gamma$  (i.e.,  $\beta_m \in [-\gamma, \gamma]$ ) affects the effectiveness of temporal randomization, we thus study the performance in thwarting Eve under distinct  $\gamma$  values. Figure 21 presents Eve’s HGR

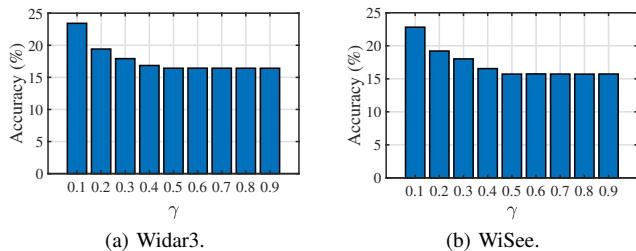


Figure 21: Gesture recognition accuracy of Eve offered by (a) Widar3 and (b) WiSee, under distinct value ranges of the randomization ratio. accuracy when the  $\gamma$  is adjusted from 0.1 to 0.9. It is

clear that, for  $\gamma$  no less than 0.5, Eve’s HGR accuracy is minimized to around 15% and remains stable in both Widar3 and WiSee models. This also corroborates our earlier choice of  $\gamma = 0.5$ .

*The Impact of Encoder Quantity.* We study how the different number of encoders impacts on MIMOCrypt. For a specific encoder quantity  $V$ , the amount of encryption matrices  $\Psi$  that the sub-model can pre-process is limited. In this section, with offering satisfactory HGR accuracy, we record the maximum quantity of  $\Psi$  being pre-processed when  $V$  is adjusted from 2 to 10. As shown in Figure 22, when  $V$  increases, the maximum quantity of  $\Psi$  varies from 4 to 86; meanwhile, the average time spent on offline model training increases apparently. As  $V$  is set as 8, the model training time is around one hour while supporting pre-process 64 encryption matrices. This might not meet our expectation (i.e.,  $2^8 = 256$ ) in Section 4.5, since the representation capacity of our implemented model (specified in Section 5) can be limited. Though a careful design of the encoders may improve the overall representation capacity of the sub-model, this is out of scope of our paper. Moreover, as we analyze in Section 4.3, one  $\Psi$  may thwart Eve for a rather long time period, so 64  $\Psi$ s is quite sufficient for MIMOCrypt’s privacy-preservation purpose.

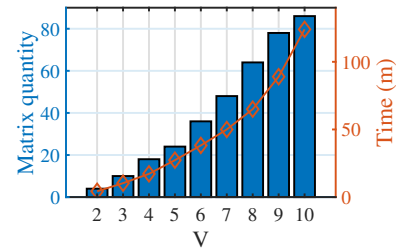


Figure 22: The encryption matrix quantity pre-processed by a sub-model and corresponding model training time cost.

## Appendix C. Future Work

*Towards General Sensing Application.* Although we take gesture recognition in this paper as an example to evaluate the performance of MIMOCrypt in thwarting Eve while protecting legitimate sensing and communication, MIMOCrypt can be easily adapted to other similar sensing applications, such as activity tracking [62] and motion recognition [4]. Its scalability stems from the following facts. First, Wi-Fi-based sensing applications share a common characteristic which they all extract features from CSI phase and amplitude via deep neural network. Consequently, MIMOCrypt can encrypt them to prevent malicious eavesdropping, no matter what the sensing applications we encounter. Second, for legitimate sensing, users only need to integrate our plug-and-play sub-model to any base recognition model. Third, for

communication services, MIMOCrypt can readily recover the LTS with the help of encryption matrices and then decode the payload data. In the future, we shall deploy MIMOCrypt into a neural network acceleration ASIC to explore the high-speed inference capability for more sensing applications.

*Compatibility with Wi-Fi Framework.* Our proposed MIMOCrypt is compatible with current Wi-Fi standards, and potentially integrated into COTS Wi-Fi chip via firmware modification. Though in this paper, we utilize the WARP SDR to build the system prototype of MIMOCrypt while evaluating its effectiveness in securing sensing and protecting communication, the WARP is widely leveraged by many researchers to verify their innovative Wi-Fi related ideas including both communication and sensing areas. We also implement our prototype strictly follows current Wi-Fi standards as the other researchers. More importantly, our source-defined encryption mechanism only involves simple encryption matrix operations. It does not need to redesign the hardware components, but only the embedded software (a.k.a firmware) in the existing COTS Wi-Fi chip. To sum up, MIMOCrypt is a promising Wi-Fi privacy-preserving

mechanism providing an innovative idea for future chip design with secure sensing considerations.

*Privacy-preserving for The Active Wi-Fi Sensing.* Different from the conventional passive Wi-Fi sensing discussed in this paper, active Wi-Fi sensing means designing special radar-like hardware that transmits Wi-Fi signals actively [63], [64]. In this way, Eve does not need to eavesdrop the signals from Alice, but generates/transmits them directly and then analyzes the reflection signals from victims to learn their activities. Recently, RF-Protect [65] leverages similar IRS technology of IRShield [18] to protect human behaviors from radar active sensing, yet it faces the same practical problem of IRShield for lack of controllability to differentiate between legitimate sensing users and attackers, as discussed in Section 2.3. Therefore, this problem can be very challenging for source-defined privacy-preserving, and we must redesign our MIMOCrypt to not only perform encrypting, but also figure out the active signals from the Eve. In the next step, we plan to explore MIMOCrypt for protecting privacy under active Wi-Fi sensing.

## Meta-Review

### Summary

The paper proposes a privacy-preserving Wi-Fi gesture recognition system called MIMOCrypt. So far, the Wi-Fi-based gesture recognition/sensing literature has allowed any Wi-Fi receiver in proximity to legitimate sensing entities also to sense the gestures. The few privacy-preserving human gesture recognition systems are incompatible with Wi-Fi standards or do not support realistic multi-user scenarios.

MIMOCrypt addresses these drawbacks and designs a multi-user privacy-preserving Wi-Fi-based human gesture recognition system without affecting legitimate communicating entities. The paper's main idea is to scramble the Wi-Fi channels at the transmitter (access point) using a "secret scrambling matrix" only known to legitimate parties, prohibiting eavesdroppers from estimating CSI changes. The paper presents an exhaustive privacy and performance evaluation of the proposed system through a proof-of-concept implementation.

### Scientific Contributions

- Provides a Valuable Step Forward in an Established Field.
- Establishes a New Research Direction.

### Reasons for Acceptance

- 1) Potentially establish a new direction in privacy-preserving wireless sensing systems.
- 2) Exhaustive experimental evaluation with a strong discussion of the results.

### Noteworthy Concerns

- 1) The need for privacy-preserving hand gesture recognition systems using Wi-Fi is not clear.

- 2) It is not clear how an attacker will be distinguished from a legitimate user.
- 3) There is a possibility that an adversary can decrypt user gestures by comparing the state of the wireless channel with and without user activity. This is a potential threat.

## Response to the Meta-Review

### Rebuttal to Noteworthy Concerns:

- 1) We believe that one thing is rather clear: as hand gesture may reveal keystrokes (in particular password typing), as suggested by a few publications cited at the end of the first paragraph in Section 1, privacy-preserving (or securing) hand gesture recognition (or general Wi-Fi sensing) is imperative.
- 2) As we have explained in Section 2.2 of our paper, whether to perform registration is a clear indication to whether a user is legitimate or not. If the concern is on "how to identify whether or not a group of users performing neural model training for Wi-Fi enabled gesture recognition are attacking MIMOCrypt via known-plaintext attack (KPA)", the answer is also clear: as no user is supposed to do so (they are supposed to use only publicly-known neural models as stated in Section 2.2), anyone attempting to do so in public should be deemed as attacking MIMOCrypt and hence should be "neutralized".
- 3) Our physical security and encryption, though different in mechanisms from their digital counterpart, work in the same vein: one cannot decrypt digital messages (resp. user gestures) by comparing two states of with or without digital message (resp. the two wireless channel states of with or without user activity). Nevertheless, as a published proposal on security defence, MIMOCrypt is open to any potential attack proposals against it, and we are ready to counteract such new proposals should they appear.